



CERN-EP-2018-217
LHCb-PAPER-2018-031
August 18, 2018

Measurement of antiproton production in pHe collisions at $\sqrt{s_{NN}} = 110 \text{ GeV}$

LHCb collaboration[†]

Abstract

The cross-section for prompt antiproton production in collisions of protons with an energy of 6.5 TeV incident on helium nuclei at rest is measured with the LHCb experiment from a data set corresponding to an integrated luminosity of 0.5 nb^{-1} . The target is provided by injecting helium gas into the LHC beam line at the LHCb interaction point. The reported results, covering antiproton momenta between 12 and 110 GeV/c, represent the first direct determination of the antiproton production cross-section in pHe collisions, and impact the interpretation of recent results on antiproton cosmic rays from space-borne experiments.

Published in Phys. Rev. Lett. 121 (2018) 222001

© 2018 CERN for the benefit of the LHCb collaboration. CC-BY-4.0 licence.

[†]Authors are listed at the end of this Letter.

The antiproton fraction in cosmic rays has been long recognized as a sensitive indirect probe for exotic astrophysical sources of antimatter, such as dark matter annihilation [1–5]. A substantial improvement in experimental accuracy for the measurement of the antiproton, \bar{p} , over proton, p , flux ratio has recently been achieved by the space-borne PAMELA [6] and AMS-02 [7] experiments. Antiproton production in spallation of cosmic rays in the interstellar medium, which is mainly composed of hydrogen and helium, is expected to produce a \bar{p}/p flux ratio of $\mathcal{O}(10^{-4})$. The observed excess of \bar{p} yields over current predictions for the known production sources [8–11] can still be accommodated within the current uncertainties. In the 10–100 GeV \bar{p} energy range, these uncertainties are dominated by the limited knowledge of the \bar{p} production cross-section in the relevant processes. To date, no direct measurements of \bar{p} production in pHe collisions have been made, and no data are available at a nucleon-nucleon center-of-mass (c.m.) energy of $\sqrt{s_{\text{NN}}} \sim 100$ GeV, relevant for the production of cosmic antiprotons above 10 GeV [12].

This Letter reports the first measurement of prompt \bar{p} production in pHe collisions carried out with the LHCb experiment at CERN using a proton beam with an energy of 6.5 TeV impinging on a helium gas target. The forward geometry and particle identification (PID) capabilities of the LHCb detector are exploited to reconstruct antiprotons with momentum, p , ranging from 12 to 110 GeV/ c and transverse momentum, p_{T} , between 0.4 and 4.0 GeV/ c . The integrated luminosity is determined from the yield of elastically scattered atomic electrons.

The LHCb detector is a single-arm forward spectrometer covering the pseudorapidity range $2 < \eta < 5$, described in detail in Refs. [13, 14], conceived for heavy-flavor physics in pp collisions at the CERN LHC. The momentum of charged particles is measured to better than 1.0% for $p < 110$ GeV/ c . The silicon-strip vertex locator (VELO), which surrounds the nominal pp interaction region, allows the measurement of the minimum distance of a track to a primary vertex (PV), the impact parameter (IP), with a resolution of $(15 + 29/p_{\text{T}})$ μm , where p_{T} is in GeV/ c . Different types of charged hadrons are distinguished using two ring-imaging Cherenkov detectors (RICH) [15], whose acceptance and performance define the \bar{p} kinematic range accessible to this study. The first RICH detector has an inner acceptance limited to $\eta < 4.4$ and is used to identify antiprotons with momenta between 12 and 60 GeV/ c . The second detector covers the range $3 < \eta < 5$ and can actively identify antiprotons with momenta between 30 and 110 GeV/ c . The scintillating-pad (SPD) detector and the electromagnetic calorimeter (ECAL) included in the calorimeter system are also used in this study.

The SMOG (System for Measuring Overlap with Gas) device [16, 17] enables the injection of noble gases with pressure of $\mathcal{O}(10^{-7})$ mbar in the beam pipe section crossing the VELO, allowing LHCb to operate as a fixed-target experiment. This analysis is performed on data specifically acquired for this measurement in May 2016. Helium gas was injected when the two beams circulating in the LHC accelerator [18] consisted of a small number, between 52 and 56, of proton bunches. The proton-beam energy of 6.5 TeV corresponds to $\sqrt{s_{\text{NN}}} = 110.5$ GeV. In the proton-nucleon c.m. frame, the LHCb acceptance corresponds to central and backward rapidities $-2.8 < y^* < 0.2$, and \bar{p} production can be studied for values of x -Feynman, the ratio of the \bar{p} longitudinal momentum to its maximal value, comprised between -0.24 and 0.

To avoid background from pp collisions, the events used for this measurement were recorded when a bunch in the beam pointing toward LHCb crosses the nominal interaction region without a corresponding colliding bunch in the other beam. The online event

selection consists of a hardware stage, which requires activity in the SPD detector, and a software stage requiring at least one reconstructed track in the VELO. An unbiased control sample of randomly selected events is acquired independently of this online selection.

Simulated data samples are generated for pHe collisions with EPOS-LHC [19], and for pe^- normalization events with ESEPP [20]. The interaction of the generated particles with the detector, and its response, are implemented using the GEANT4 toolkit [21] as described in Ref. [22]. Simulated collisions are uniformly distributed along the nominal beam direction z in the range $-1000 < z < +300$ mm, where $z = 0$ mm is the nominal collision point.

Events with antiproton candidates must have a reconstructed primary vertex within the fiducial region $-700 < z_{PV} < +100$ mm, where high reconstruction efficiencies are achieved for both pHe and pe^- collisions. The PV position must be compatible with the beam profile and events must have fewer than 5 tracks reconstructed in the VELO with negative pseudorapidity. This selection is $(99.8 \pm 0.2)\%$ efficient for simulated reconstructed pHe vertices, while suppressing vertices from interactions with material, decays, and particle showers produced in beam-gas collisions occurring upstream of the VELO. The overlap of these backgrounds with a pHe collision, an effect not accounted for by the simulation, causes an additional inefficiency of $(2.3 \pm 0.2)\%$, measured using the unbiased control sample. The PV reconstruction efficiency for the signal events is estimated from simulation and varies with z_{PV} from 66% in the most upstream region to 97% around $z_{PV} = 0$ mm. This efficiency is sensitive to the PV track multiplicity, the angular distribution of primary tracks and the average position and profile of the beam. Imperfections in these simulated distributions are accounted for by weighting simulated events to improve the agreement with the distributions observed in data. From the resulting variations of the PV reconstruction efficiency, a relative systematic uncertainty is assigned, ranging from 1.6% to 3.3%, depending on the \bar{p} kinematics.

Antiproton candidates are selected from negatively charged tracks within the acceptance of at least one of the RICH detectors. Additionally, \bar{p} candidates are required to originate from the primary vertex by requiring $\chi_{IP}^2 < 12$, where χ_{IP}^2 is defined as the difference in the vertex-fit χ^2 of the PV reconstructed with and without the track under consideration. The reconstruction efficiency for prompt antiprotons, ϵ_{rec} , including the detector acceptance and the tracking efficiency, is determined from simulation in three-dimensional bins of p , p_T and z_{PV} . The width of the momentum bins increases as a power law of p to have approximately an equal number of candidates in each of 18 bins. Ten p_T bins are chosen with the same criterion, while 12 uniform bins are used in z_{PV} . Bins in which ϵ_{rec} is below 25% are not used in order to reduce systematic uncertainties, effectively shortening the z_{PV} fiducial region for kinematic bins at the edges of the detector acceptance. The average value of ϵ_{rec} in the remaining bins is 61%. The tracking efficiency obtained from the simulation is corrected by a factor determined from calibration samples in pp-collision data. This correction factor is consistent with unity in all kinematic bins within its systematic uncertainty of 0.8% [23]. The z_{PV} dependence of the tracking efficiency is checked using $K_S^0 \rightarrow \pi^+\pi^-$ decays in the pHe sample where one of the tracks is reconstructed without using VELO information. No significant differences between data and simulation are observed. A systematic uncertainty, varying between 1.0% and 4.0% depending on η , accounts for \bar{p} hadronic interactions in the detector material, whose rate is known with 10% accuracy [23]. The efficiency of the χ_{IP}^2 requirement is parameterized as a function of p_T and p , averaging to 96.1%, with a 1.0% uncertainty from the parameterization

accuracy. The online selection efficiency is unity, within 10^{-5} , as determined from the unbiased control sample.

Based on studies of simulated pHe collisions, the sample of negatively charged tracks is dominated by π^- , K^- and \bar{p} hadrons. In a small fraction of cases, 1.7% in the simulation, tracks do not correspond to the trajectories of real charged particles and are labelled as fake tracks. Particle identification is based on the response of the RICH detectors, from which two quantities are determined: the difference between the log likelihood of the proton and pion hypotheses, $DLL_{p\pi}$, and that between the proton and kaon hypotheses, DLL_{pK} [15]. Three sets of templates for each particle species are determined from simulation, from pHe data, and from pp data collected in 2016. The pHe calibration samples consist of selected $K_S^0 \rightarrow \pi^+\pi^-$ decays for pions, $\Lambda \rightarrow p\pi^-$ ($\bar{\Lambda} \rightarrow \bar{p}\pi^+$) for (anti)protons and $\phi \rightarrow K^+K^-$ for kaons. Calibration samples in pp data also include $D^{*\pm} \rightarrow \bar{D}^0(K^\mp\pi^\pm)\pi^\pm$ decays. Simulation is used for the template of fake tracks.

Two methods are used to determine the \bar{p} fraction in each kinematic bin: a two-dimensional binned extended-maximum-likelihood fit, illustrated in Fig. 1, and a cut-and-count method [24], which uses exclusive high-purity samples selected with tight requirements for each particle species. The probability P_{ij} that a candidate of species i is classified as species j is obtained from the templates. The 4×4 P_{ij} matrix is then inverted to derive the yield of each particle species. For each kinematic bin, the central value for the \bar{p} fraction is obtained from the average of the two methods using the templates from simulation, while half the difference is used to estimate the systematic uncertainty. Bias from the imperfections of the simulated RICH response, which are visible in Fig. 1, is estimated from the average differences among the results using the three available template sets, which are used to assign an additional uncertainty, correlated among bins. The total uncertainty is typically a few percent, although larger uncertainties affect the bins at the edges of the detector acceptance.

In the simulation, the non-prompt antiprotons surviving the χ_{IP}^2 requirement constitute a fraction of the selected \bar{p} sample varying between 1% and 3% depending on p_T . These are due to hyperon decays, in 90% of cases, or secondary interactions. This fraction is corrected by a factor 1.5 ± 0.3 , to account for differences between simulation and data as determined in the region of the χ_{IP}^2 distribution dominated by hyperon decays. The resulting correction to the \bar{p} yield averages to -2.4% .

Collisions on the residual gas in the LHC beam vacuum, with a pressure of $\mathcal{O}(10^{-9})$ mbar and unknown composition, can contribute to the \bar{p} yield. Residual-gas analysis, performed in the absence of beam, indicates that the contamination is $\mathcal{O}(1)\%$ and is dominated by hydrogen. To evaluate this background source, including a possible beam-induced component, a control sample of beam-gas collisions was acquired before injection of the helium gas. Data collected with and without helium gas have the same vacuum pumping configuration and thus identical residual gas composition and pressure. The yield of selected events in data without helium gas, scaled according to the corresponding number of protons on target, is subtracted from the result leading to an average correction of $(-0.6 \pm 0.1)\%$, where the uncertainty accounts for the background variation over time. The average PV track multiplicity is found to be smaller in collisions without injected gas, confirming that the residual gas is dominated by hydrogen.

Since the injected gas pressure is not precisely known, the integrated luminosity of the data sample is determined from the yield of electrons from elastic scattering of the proton beam. Scattered electrons are simulated in the polar angle range $3 < \theta < 27$ mrad,

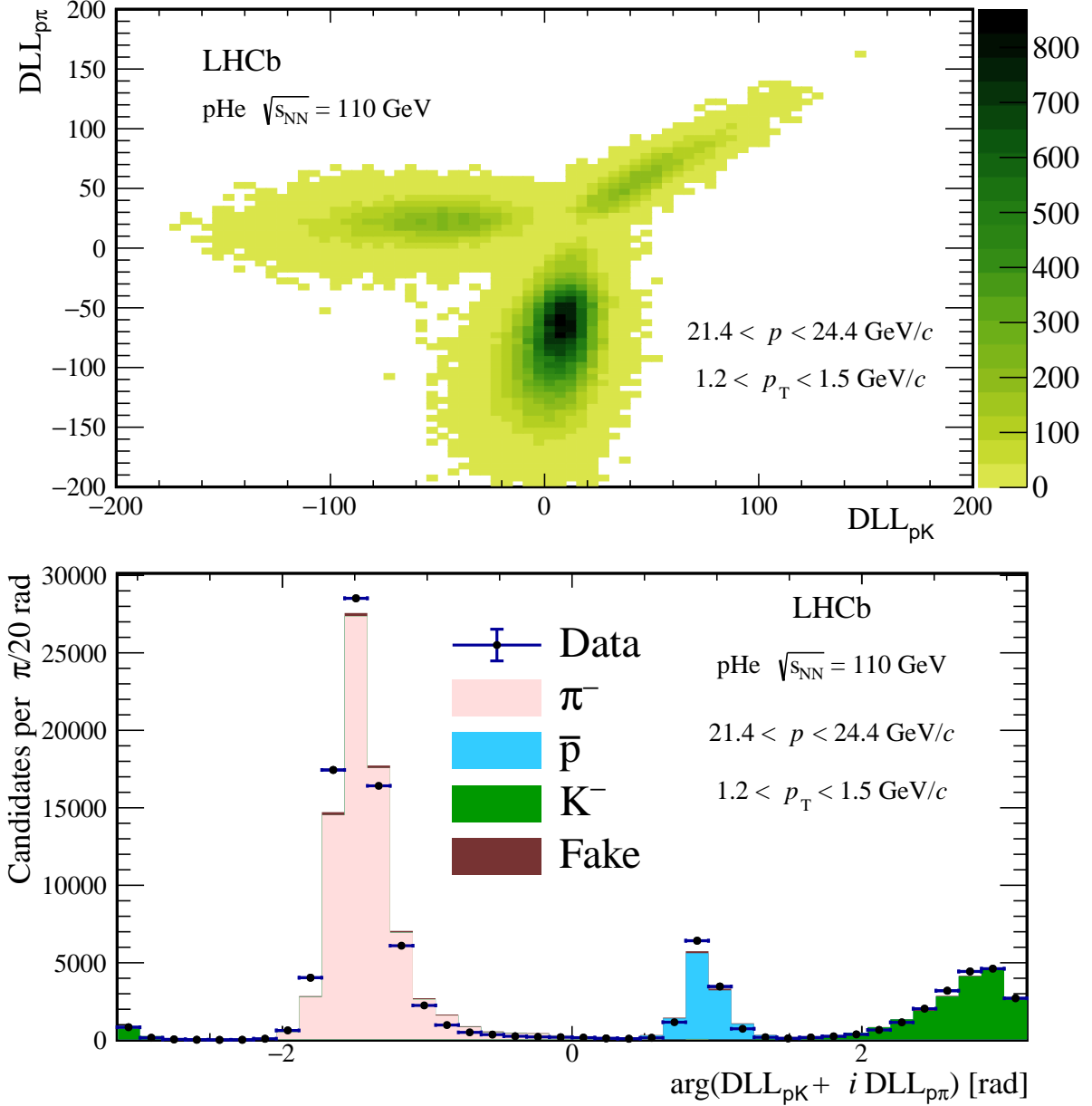


Figure 1: Two-dimensional template fit to the PID distribution of negatively charged tracks for a particular bin ($21.4 < p < 24.4$ GeV/c, $1.2 < p_T < 1.5$ GeV/c). The $(DLL_{pK}, DLL_{p\pi})$ distribution, shown in the top plot, is fitted to determine the relative contribution of π^- , K^- and \bar{p} particles, using simulation to determine the template distributions and the fraction of fake tracks (which are barely visible). In the bottom plot, the result of the fit is projected into the variable $\arg(DLL_{pK} + i DLL_{p\pi})$.

outside of which they cannot be reconstructed in LHCb. The corresponding cross-section is calculated to be 184.8 ± 1.8 μb [20], where the uncertainty is due to the proton form factors and radiative corrections. Scattered electrons are selected from events with a single reconstructed track. The electron candidate is required to have $p < 15$ GeV/c, $p_T < 0.12$ GeV/c, a polar angle in the range $11 < \theta < 21$ mrad, and to originate from the fiducial region. The longitudinal position of the scattering vertex z_{pe^-} is determined from

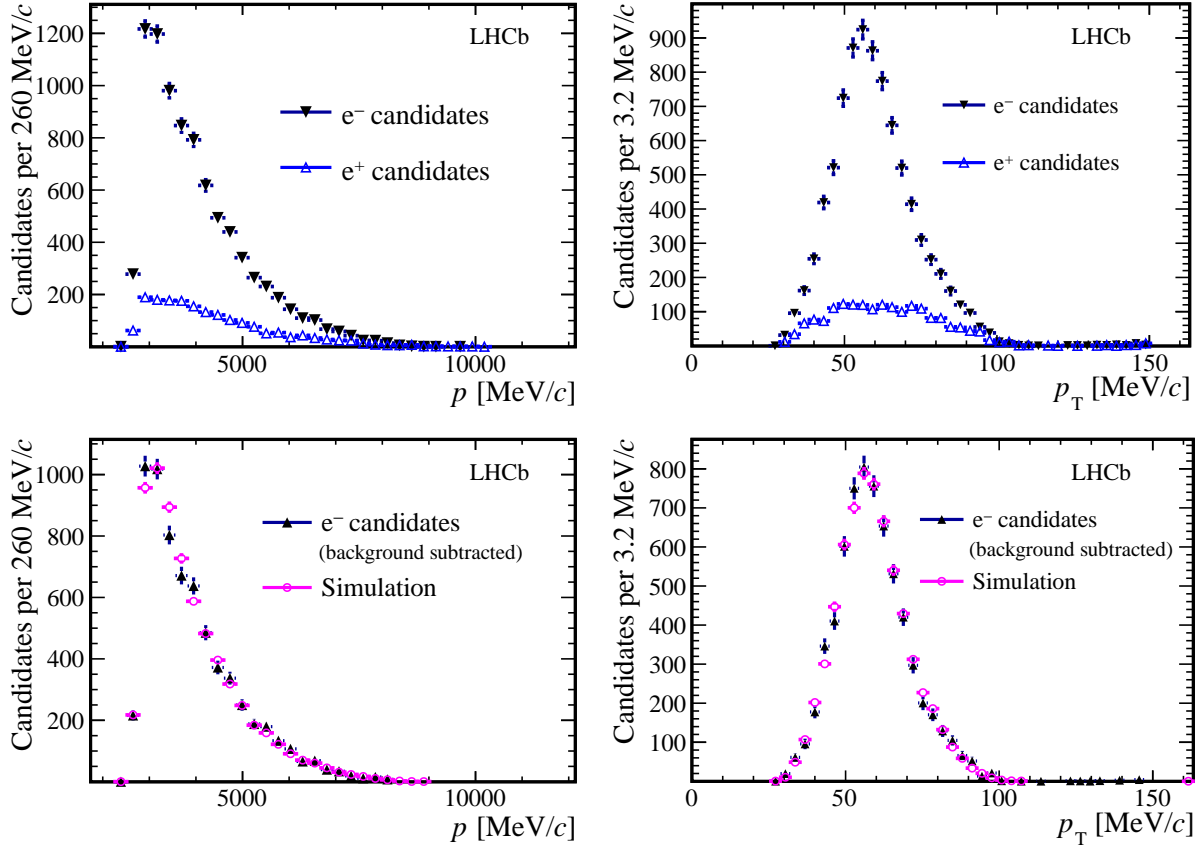


Figure 2: Distributions of (left) momentum and (right) transverse momentum for (top) single electron and single positron candidates, and (bottom) background-subtracted electron candidates, compared with the distributions in simulation, which are normalized to the data yield.

the position of minimum approach to the beam line, with a resolution of 9 cm. The track reconstruction efficiency in the selected z_{pe^-} and θ ranges is determined from simulation to be 16.3%. A loose requirement is placed on the energy deposited in the ECAL to identify the track as an electron. Background events that could mimic this signature are expected to be mostly soft nuclear collisions where the initial nucleons do not dissociate, and the detected particle is produced by a colorless exchange of gluons or photons. Since the products of this process must be charge-symmetric, the background yield is determined from events with a single positron candidate.

Background is further suppressed by two multivariate classifiers, implemented using a BDT algorithm [25]. The first exploits the geometric and kinematic properties of the candidate electron. The second uses multiplicity variables to veto any extra activity in the event. In both cases the classifiers are trained using pe^- simulated events for the signal and single-positron events from data for the background. Loose requirements are placed on the response of the BDT discriminants, with a combined efficiency of 96% for simulated pe^- events. The overlap of a pe^- event with another beam-gas interaction causes an additional inefficiency, measured to be $(9.4 \pm 0.7)\%$ in the unbiased control sample. A possible charge asymmetry of the background, estimated from the EPOS simulation, leads to a systematic uncertainty of 1.9%. As is done for the \bar{p} candidates, the unbiased control events are used to measure the online selection efficiency, $(98.3 \pm 0.3)\%$, and the data

without helium gas are used to determine the contribution from scattering on residual gas, $(1.0 \pm 0.3)\%$.

The momentum distributions of the selected candidates are shown in Fig. 2, where a good agreement with the simulated pe^- signal is observed after background subtraction. The low reconstruction efficiency, due to the fact that the observed electrons are predominantly produced at the edges of the LHCb acceptance and are subject to relevant energy losses by bremsstrahlung when crossing the detector material, is the major source of systematic uncertainty on the luminosity. The stability of the result is checked against additional requirements on the most critical variables, notably the number of reconstructed VELO hits and the azimuthal angle, whose distribution is strongly affected by the spectrometer magnetic field. The largest variation of the result, a relative 5.0%, is assigned as systematic uncertainty on the electron reconstruction efficiency. Taking also into account an uncertainty of 2.3% from the beam and VELO simulated geometry, the total systematic uncertainty on the luminosity is 6.0%.

The integrated pHe luminosity is determined from the efficiency-corrected yield, divided by the product of the pe^- cross-section and the helium atomic number. Gas ionization effects are found to be negligible. Avoiding any assumption on the z dependence of the gas density, the integrated luminosity is calculated with 12 z_{pe^-} -bins across the fiducial region, resulting in $484 \pm 7 \pm 29 \mu\text{b}^{-1}$, where the first uncertainty is statistical and the second is systematic. From the knowledge of the number of delivered protons, the target gas pressure is found to be 2.6×10^{-7} mbar, which is compatible with the expected helium pressure.

Table 1 presents the list of uncertainties on the \bar{p} cross-section measurement, categorized into correlated and uncorrelated sources among kinematic bins. The correlated systematic uncertainty is dominated by the uncertainty on the luminosity determination. The net

Table 1: Relative uncertainties on the \bar{p} production cross-section. The ranges refer to the variation among kinematic bins.

Statistical	
\bar{p} yields	0.5 – 11% (< 2% for most bins)
Luminosity	1.5 – 2.3%
Correlated systematic	
Luminosity	6.0%
Event and PV selection	0.3%
PV reconstruction	0.4 – 2.9%
Tracking	1.3 – 4.1%
Non-prompt background	0.3 – 0.5%
Target purity	0.1%
PID	3.0 – 6.0%
Uncorrelated systematic	
Tracking	1.0%
IP cut efficiency	1.0%
PV reconstruction	1.6%
PID	0 – 36% (< 5% for most bins)
Simulated sample size	0.4 – 11% (< 2% for most bins)

effect of migration between kinematic bins due to resolution effects is found to be negligible. A major difference between the fixed-target configuration and the standard pp-collision data taking in LHCb is the extension of the luminous region. As a consequence, the result is checked to be independent of z_{PV} within the quoted uncertainty in all kinematic bins. Furthermore, the results do not show any significant dependence on the time of data taking.

The \bar{p} production cross-section is determined in each kinematic bin from a sample of 33.7 million reconstructed pHe collisions, yielding 1.5 million antiprotons as determined from the PID analysis. In Fig. 3, the results, integrated in different kinematic regions, are compared with the prediction of several models: EPOS-LHC [19], the pre-LHC EPOS version 1.99 [26], HIJING 1.38 [27], the QGSJET model II-04 [28] and its low-energy extension QGSJETII-04m, motivated by \bar{p} production in cosmic rays [29]. The results are also compared with the PYTHIA6.4 [30] prediction for $2 \times [\sigma(\text{pp} \rightarrow \bar{p}X) + \sigma(\text{pn} \rightarrow \bar{p}X)]$, not including nuclear effects. The shapes are well reproduced except at low rapidity, and the absolute \bar{p} yields deviate by up to a factor of two. Numerical values for the double-differential cross-section $d^2\sigma/dp dp_T$ in each kinematic bin are available in Appendix A.

The total yield of pHe inelastic collisions which are visible in LHCb is determined from the yield of reconstructed primary vertices and is found to be compatible with EPOS-LHC: $\sigma_{\text{vis}}^{\text{LHCb}}/\sigma_{\text{vis}}^{\text{EPOS-LHC}} = 1.08 \pm 0.07 \pm 0.03$, where the first uncertainty is due to the luminosity and the second to the PV reconstruction efficiency. The result indicates that the significant excess of \bar{p} production over the EPOS-LHC prediction, visible in Fig. 3, is mostly due to the \bar{p} multiplicity.

In summary, using a pHe collision data sample, corresponding to an integrated luminosity of 0.5 nb^{-1} , the LHCb collaboration has performed the first measurement of antiproton production in pHe collisions. The precision is limited by systematic effects and is better than a relative 10% for most kinematic bins, well below the spread among models describing \bar{p} production in nuclear collisions. The energy scale, $\sqrt{s_{\text{NN}}} = 110 \text{ GeV}$, and the measured range of the antiproton kinematic spectrum are crucial for interpreting the precise \bar{p} cosmic ray measurements from the PAMELA and AMS-02 experiments by improving the precision of the secondary \bar{p} cosmic ray flux prediction [11, 31].

Acknowledgements

We are grateful to our colleagues from the cosmic ray community, O. Adriani, F. Donato, L. Bonechi and A. Tricomi, for suggesting this measurement, to T. Pierog and S. Ostapchenko for their advice on the theoretical models for antiproton production, and to B. Ward and A. V. Gramolin for their advice on the model and uncertainty for pe^- scattering. We express our gratitude to our colleagues in the CERN accelerator departments for the excellent performance of the LHC. We thank the technical and administrative staff at the LHCb institutes. We acknowledge support from CERN and from the national agencies: CAPES, CNPq, FAPERJ and FINEP (Brazil); MOST and NSFC (China); CNRS/IN2P3 (France); BMBF, DFG and MPG (Germany); INFN (Italy); NWO (Netherlands); MNiSW and NCN (Poland); MEN/IFA (Romania); MSHE (Russia); MinECo (Spain); SNSF and SER (Switzerland); NASU (Ukraine); STFC (United Kingdom); NSF (USA). We acknowledge the computing resources that are provided by CERN, IN2P3 (France), KIT and DESY (Germany), INFN (Italy), SURF (Netherlands), PIC (Spain), GridPP (United

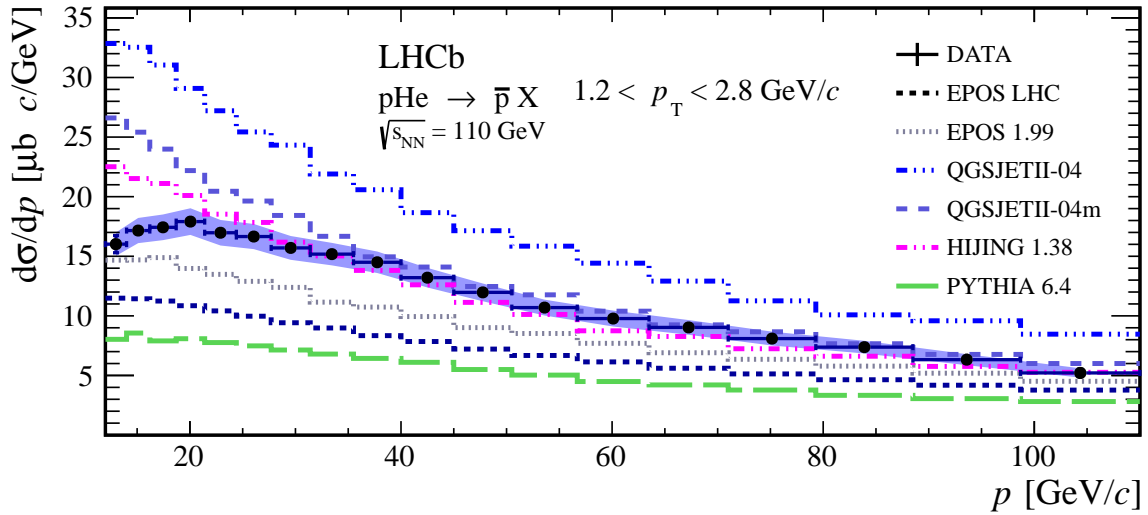
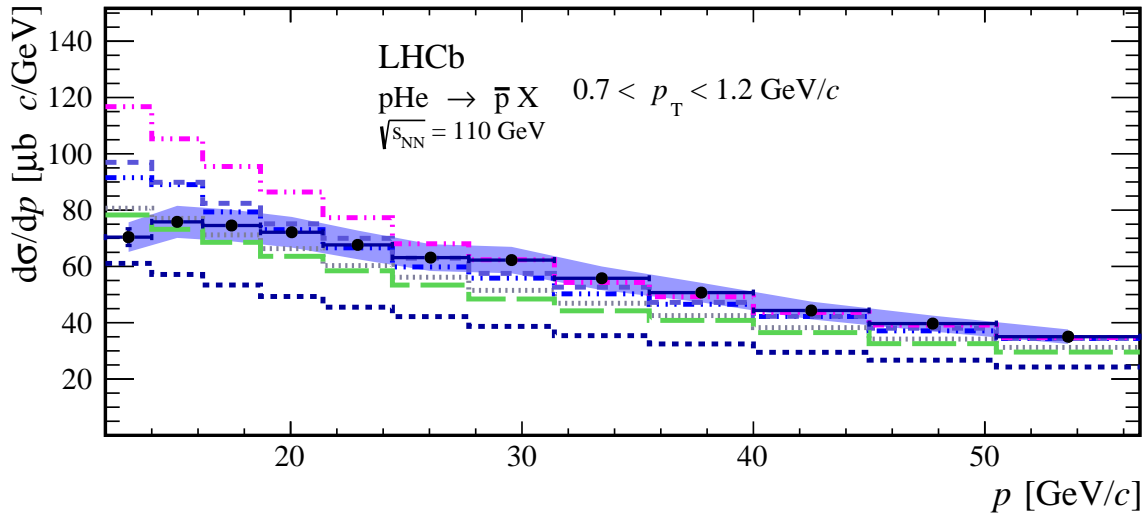
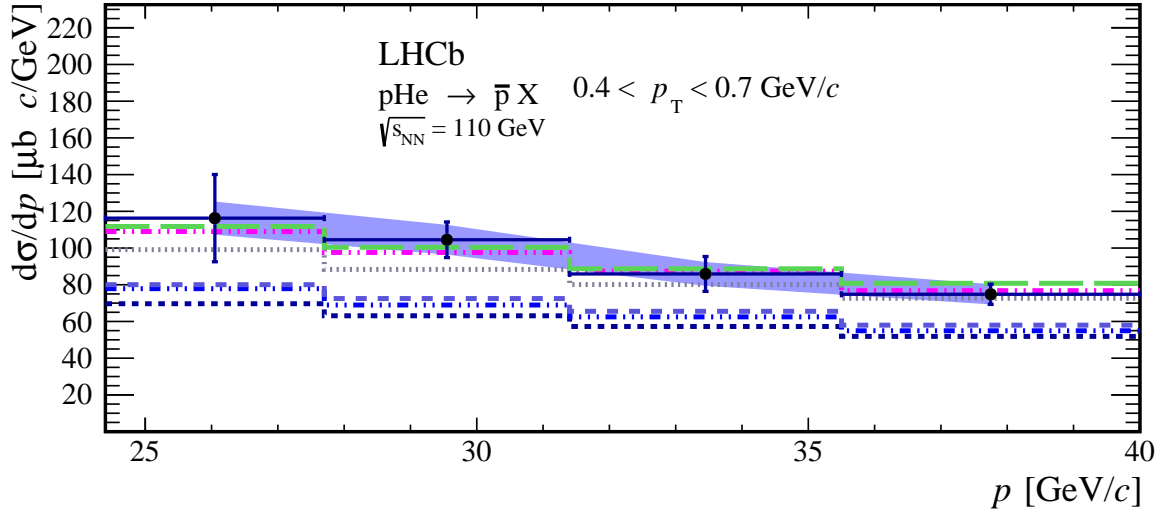


Figure 3: Antiproton production cross-section per He nucleus as a function of momentum, integrated over various p_T regions. The data points are compared with predictions from theoretical models. The uncertainties on the data points are uncorrelated only, while the shaded area indicates the correlated uncertainty.

Kingdom), RRCKI and Yandex LLC (Russia), CSCS (Switzerland), IFIN-HH (Romania), CBPF (Brazil), PL-GRID (Poland) and OSC (USA). We are indebted to the communities behind the multiple open-source software packages on which we depend. Individual groups or members have received support from AvH Foundation (Germany); EPLANET, Marie Skłodowska-Curie Actions and ERC (European Union); ANR, Labex P2IO and OCEVU, and Région Auvergne-Rhône-Alpes (France); Key Research Program of Frontier Sciences of CAS, CAS PIFI, and the Thousand Talents Program (China); RFBR, RSF and Yandex LLC (Russia); GVA, XuntaGal and GENCAT (Spain); the Royal Society and the Leverhulme Trust (United Kingdom); Laboratory Directed Research and Development program of LANL (USA).

A Numerical results

The numerical results for the antiproton production cross-section per He nucleus in pHe collisions at $\sqrt{s_{\text{NN}}} = 110$ GeV are reported in Table 2 for each kinematic bin.

The cross-section for pHe inelastic collisions whose primary vertex can be reconstructed in LHCb (at least three primary tracks within the acceptance of the VELO detector) is measured to be

$$\sigma_{\text{vis}}^{\text{LHCb}} = (71.9 \pm 4.5 \pm 2.3) \text{ mb},$$

where the first uncertainty is due to the luminosity and the second to the reconstruction efficiency. The EPOS-LHC prediction is 66.6 mb for this visible cross-section, and 118 mb for the total inelastic cross-section. The fraction of events not reconstructible in LHCb varies between 33 and 44% among the EPOS-LHC, QGSJETII-04 and HIJING models.

Table 2: Numerical results for the measured prompt \bar{p} production cross-section. The reported values are the double-differential cross-section $d^2\sigma/dp dp_T$ per He nucleus in the laboratory frame, averaged over the given kinematic range of each bin. The uncertainty is split into an uncorrelated uncertainty δ_{uncorr} , and an uncertainty δ_{corr} which is fully correlated among the kinematic bins. For both uncertainties, the systematic uncertainty, dominant for most bins, and the statistical uncertainty, are added in quadrature. The average value within each bin is also reported for p , p_T and x -Feynman $x_F = 2p_Z^*/\sqrt{s_{\text{NN}}}$, where p_Z^* is the longitudinal \bar{p} momentum in the proton-nucleon center-of-mass system. These average values are obtained from simulation, to avoid biases from reconstruction effects and given the good agreement with data observed for the simulated kinematic spectra.

p range	p_T range	$\langle p \rangle$	$\langle p_T \rangle$	$\langle x_F \rangle$	$\frac{d^2\sigma}{dp dp_T}$	δ_{uncorr}	δ_{corr}
[GeV/c]	[GeV/c]	[GeV/c]	[GeV/c]		$\left[\frac{\mu\text{b} c^2}{\text{GeV}^2}\right]$	$\left[\frac{\mu\text{b} c^2}{\text{GeV}^2}\right]$	$\left[\frac{\mu\text{b} c^2}{\text{GeV}^2}\right]$
12.0 – 14.0	0.6 – 0.7	12.99	0.62	−0.050	324	7	26
12.0 – 14.0	0.7 – 0.8	12.99	0.75	−0.057	241	27	19
12.0 – 14.0	0.8 – 0.9	12.99	0.85	−0.063	188	22	15
12.0 – 14.0	0.9 – 1.1	12.99	0.97	−0.073	122	15	10
12.0 – 14.0	1.1 – 1.2	12.99	1.12	−0.085	80	10	5
12.0 – 14.0	1.2 – 1.5	12.99	1.32	−0.106	38.5	2.7	2.6
12.0 – 14.0	1.5 – 2.0	12.99	1.67	−0.149	8.7	0.7	0.6
12.0 – 14.0	2.0 – 2.8	12.99	2.21	−0.236	0.77	0.11	0.05
14.0 – 16.2	0.6 – 0.7	15.09	0.62	−0.042	312	7	25
14.0 – 16.2	0.7 – 0.8	15.09	0.75	−0.048	245	7	20
14.0 – 16.2	0.8 – 0.9	15.09	0.85	−0.054	195.1	4.9	15.4
14.0 – 16.2	0.9 – 1.1	15.09	0.97	−0.062	135.2	3.4	10.6
14.0 – 16.2	1.1 – 1.2	15.09	1.12	−0.073	80.9	3.1	5.4
14.0 – 16.2	1.2 – 1.5	15.09	1.32	−0.091	40.0	1.3	2.6
14.0 – 16.2	1.5 – 2.0	15.09	1.67	−0.128	9.33	0.39	0.62
14.0 – 16.2	2.0 – 2.8	15.09	2.21	−0.202	1.10	0.11	0.07

p range	p_T range	$\langle p \rangle$	$\langle p_T \rangle$	$\langle x_F \rangle$	$\frac{d^2\sigma}{dp dp_T}$	δ_{uncorr}	δ_{corr}
[GeV/c]	[GeV/c]	[GeV/c]	[GeV/c]		$\left[\frac{\mu\text{b}c^2}{\text{GeV}^2}\right]$	$\left[\frac{\mu\text{b}c^2}{\text{GeV}^2}\right]$	$\left[\frac{\mu\text{b}c^2}{\text{GeV}^2}\right]$
16.2 – 18.7	0.6 – 0.7	17.43	0.62	–0.036	281	10	22
16.2 – 18.7	0.7 – 0.8	17.43	0.75	–0.041	234	6	19
16.2 – 18.7	0.8 – 0.9	17.43	0.85	–0.046	190.2	4.7	15.1
16.2 – 18.7	0.9 – 1.1	17.43	0.97	–0.053	133.5	3.3	10.6
16.2 – 18.7	1.1 – 1.2	17.43	1.12	–0.062	81.0	2.2	5.4
16.2 – 18.7	1.2 – 1.5	17.43	1.32	–0.078	39.2	1.1	2.6
16.2 – 18.7	1.5 – 2.0	17.43	1.68	–0.110	10.44	0.40	0.69
16.2 – 18.7	2.0 – 2.8	17.43	2.21	–0.174	1.03	0.09	0.07
18.7 – 21.4	0.6 – 0.7	20.03	0.62	–0.031	277	19	22
18.7 – 21.4	0.7 – 0.8	20.03	0.75	–0.035	221	5	18
18.7 – 21.4	0.8 – 0.9	20.03	0.85	–0.039	179.1	4.5	14.2
18.7 – 21.4	0.9 – 1.1	20.03	0.97	–0.045	128.3	3.2	10.2
18.7 – 21.4	1.1 – 1.2	20.03	1.12	–0.054	82.2	2.2	5.5
18.7 – 21.4	1.2 – 1.5	20.03	1.32	–0.067	40.1	1.1	2.7
18.7 – 21.4	1.5 – 2.0	20.03	1.68	–0.095	10.44	0.39	0.69
18.7 – 21.4	2.0 – 2.8	20.03	2.22	–0.151	1.16	0.08	0.07
21.4 – 24.4	0.6 – 0.7	22.88	0.62	–0.026	278	6	22
21.4 – 24.4	0.7 – 0.8	22.88	0.75	–0.030	213	5	17
21.4 – 24.4	0.8 – 0.9	22.88	0.85	–0.034	167.2	4.2	13.3
21.4 – 24.4	0.9 – 1.1	22.88	0.97	–0.039	119.5	3.0	9.5
21.4 – 24.4	1.1 – 1.2	22.88	1.12	–0.046	78.0	2.1	5.3
21.4 – 24.4	1.2 – 1.5	22.88	1.32	–0.058	37.7	1.1	2.6
21.4 – 24.4	1.5 – 2.0	22.88	1.68	–0.083	10.38	0.36	0.68
21.4 – 24.4	2.0 – 2.8	22.88	2.22	–0.132	1.19	0.09	0.08
24.4 – 27.7	0.4 – 0.6	26.02	0.47	–0.019	519	185	44
24.4 – 27.7	0.6 – 0.7	26.02	0.62	–0.022	289	13	24
24.4 – 27.7	0.7 – 0.8	26.02	0.75	–0.025	205	5	16
24.4 – 27.7	0.8 – 0.9	26.02	0.85	–0.029	156.2	3.9	12.4
24.4 – 27.7	0.9 – 1.1	26.02	0.97	–0.033	110.6	2.7	8.8
24.4 – 27.7	1.1 – 1.2	26.02	1.12	–0.040	72.8	1.9	4.9
24.4 – 27.7	1.2 – 1.5	26.02	1.32	–0.050	37.0	1.0	2.5
24.4 – 27.7	1.5 – 2.0	26.02	1.68	–0.072	9.94	0.33	0.67
24.4 – 27.7	2.0 – 2.8	26.02	2.23	–0.116	1.29	0.08	0.08
27.7 – 31.4	0.4 – 0.6	29.52	0.47	–0.015	451	116	38
27.7 – 31.4	0.6 – 0.7	29.52	0.62	–0.018	318	45	27
27.7 – 31.4	0.7 – 0.8	29.52	0.75	–0.021	219	5	18
27.7 – 31.4	0.8 – 0.9	29.52	0.85	–0.024	152.2	3.8	12.2
27.7 – 31.4	0.9 – 1.1	29.52	0.97	–0.028	103.5	2.6	8.2
27.7 – 31.4	1.1 – 1.2	29.52	1.12	–0.034	67.8	1.8	4.6
27.7 – 31.4	1.2 – 1.5	29.52	1.33	–0.043	33.9	1.0	2.3
27.7 – 31.4	1.5 – 2.0	29.52	1.68	–0.062	9.89	0.32	0.67
27.7 – 31.4	2.0 – 2.8	29.52	2.23	–0.101	1.28	0.08	0.08

p range	p_T range	$\langle p \rangle$	$\langle p_T \rangle$	$\langle x_F \rangle$	$\frac{d^2\sigma}{dp dp_T}$	δ_{uncorr}	δ_{corr}
[GeV/c]	[GeV/c]	[GeV/c]	[GeV/c]		$\left[\frac{\mu\text{b}c^2}{\text{GeV}^2}\right]$	$\left[\frac{\mu\text{b}c^2}{\text{GeV}^2}\right]$	$\left[\frac{\mu\text{b}c^2}{\text{GeV}^2}\right]$
31.4 – 35.5	0.4 – 0.6	33.41	0.47	–0.012	339	75	31
31.4 – 35.5	0.6 – 0.7	33.41	0.62	–0.015	274	54	23
31.4 – 35.5	0.7 – 0.8	33.41	0.75	–0.018	195	15	16
31.4 – 35.5	0.8 – 0.9	33.41	0.85	–0.020	136.4	3.7	11.0
31.4 – 35.5	0.9 – 1.1	33.41	0.97	–0.024	95.0	2.4	7.6
31.4 – 35.5	1.1 – 1.2	33.41	1.12	–0.029	62.5	1.7	4.2
31.4 – 35.5	1.2 – 1.5	33.41	1.33	–0.037	32.0	0.9	2.2
31.4 – 35.5	1.5 – 2.0	33.41	1.68	–0.054	9.58	0.31	0.64
31.4 – 35.5	2.0 – 2.8	33.41	2.23	–0.088	1.40	0.07	0.09
35.5 – 40.0	0.4 – 0.6	37.71	0.47	–0.010	267	39	25
35.5 – 40.0	0.6 – 0.7	37.71	0.62	–0.012	240	11	21
35.5 – 40.0	0.7 – 0.8	37.71	0.75	–0.015	177	13	16
35.5 – 40.0	0.8 – 0.9	37.71	0.85	–0.017	125.1	3.3	10.9
35.5 – 40.0	0.9 – 1.1	37.71	0.97	–0.020	86.9	2.2	6.0
35.5 – 40.0	1.1 – 1.2	37.71	1.12	–0.024	57.7	1.6	3.9
35.5 – 40.0	1.2 – 1.5	37.71	1.33	–0.032	30.6	0.8	2.1
35.5 – 40.0	1.5 – 2.0	37.71	1.68	–0.047	9.11	0.29	0.61
35.5 – 40.0	2.0 – 2.8	37.71	2.23	–0.077	1.34	0.07	0.09
35.5 – 40.0	2.8 – 4.0	37.71	3.06	–0.139	0.065	0.012	0.004
40.0 – 45.0	0.6 – 0.7	42.46	0.62	–0.009	192	12	17
40.0 – 45.0	0.7 – 0.8	42.46	0.75	–0.012	148	5	13
40.0 – 45.0	0.8 – 0.9	42.46	0.85	–0.014	110	7	10
40.0 – 45.0	0.9 – 1.1	42.46	0.97	–0.016	79.4	2.1	6.9
40.0 – 45.0	1.1 – 1.2	42.46	1.12	–0.020	49.8	1.4	3.4
40.0 – 45.0	1.2 – 1.5	42.46	1.33	–0.027	27.4	0.7	1.8
40.0 – 45.0	1.5 – 2.0	42.46	1.69	–0.040	8.79	0.27	0.59
40.0 – 45.0	2.0 – 2.8	42.46	2.24	–0.067	1.26	0.06	0.08
40.0 – 45.0	2.8 – 4.0	42.46	3.08	–0.124	0.059	0.010	0.004
45.0 – 50.5	0.6 – 0.7	47.70	0.62	–0.007	151.4	3.9	14.0
45.0 – 50.5	0.7 – 0.8	47.70	0.75	–0.009	130.0	3.4	11.5
45.0 – 50.5	0.8 – 0.9	47.70	0.85	–0.011	100.8	3.4	9.0
45.0 – 50.5	0.9 – 1.1	47.70	0.97	–0.013	70.8	1.9	6.3
45.0 – 50.5	1.1 – 1.2	47.70	1.12	–0.016	45.5	2.4	3.2
45.0 – 50.5	1.2 – 1.5	47.70	1.33	–0.022	23.7	0.6	1.6
45.0 – 50.5	1.5 – 2.0	47.70	1.69	–0.034	8.38	0.26	0.56
45.0 – 50.5	2.0 – 2.8	47.70	2.24	–0.058	1.29	0.06	0.09
45.0 – 50.5	2.8 – 4.0	47.70	3.09	–0.109	0.059	0.009	0.004
50.5 – 56.7	0.7 – 0.8	53.54	0.75	–0.006	109.2	3.1	9.9
50.5 – 56.7	0.8 – 0.9	53.54	0.85	–0.008	86.6	2.4	7.6
50.5 – 56.7	0.9 – 1.1	53.54	0.97	–0.010	65.8	1.8	5.8
50.5 – 56.7	1.1 – 1.2	53.54	1.12	–0.013	40.3	1.2	3.5
50.5 – 56.7	1.2 – 1.5	53.54	1.33	–0.018	21.0	0.7	1.5
50.5 – 56.7	1.5 – 2.0	53.54	1.69	–0.029	7.56	0.23	0.51
50.5 – 56.7	2.0 – 2.8	53.54	2.24	–0.051	1.18	0.05	0.08
50.5 – 56.7	2.8 – 4.0	53.54	3.09	–0.096	0.070	0.010	0.005

p range	p_T range	$\langle p \rangle$	$\langle p_T \rangle$	$\langle x_F \rangle$	$\frac{d^2\sigma}{dp dp_T}$	δ_{uncorr}	δ_{corr}
[GeV/c]	[GeV/c]	[GeV/c]	[GeV/c]		$\left[\frac{\mu\text{b}c^2}{\text{GeV}^2}\right]$	$\left[\frac{\mu\text{b}c^2}{\text{GeV}^2}\right]$	$\left[\frac{\mu\text{b}c^2}{\text{GeV}^2}\right]$
56.7 – 63.5	0.8 – 0.9	60.04	0.85	–0.005	74.1	2.2	6.6
56.7 – 63.5	0.9 – 1.1	60.04	0.97	–0.007	57.8	1.6	5.1
56.7 – 63.5	1.1 – 1.2	60.04	1.12	–0.010	37.0	1.1	3.3
56.7 – 63.5	1.2 – 1.5	60.04	1.33	–0.014	18.7	0.5	1.6
56.7 – 63.5	1.5 – 2.0	60.04	1.69	–0.024	6.79	0.21	0.46
56.7 – 63.5	2.0 – 2.8	60.04	2.24	–0.043	1.22	0.06	0.08
56.7 – 63.5	2.8 – 4.0	60.04	3.09	–0.083	0.071	0.010	0.005
63.5 – 71.0	0.8 – 0.9	67.18	0.85	–0.002	64.6	2.4	6.2
63.5 – 71.0	0.9 – 1.1	67.18	0.97	–0.004	51.7	1.5	4.6
63.5 – 71.0	1.1 – 1.2	67.18	1.12	–0.007	35.2	1.1	3.1
63.5 – 71.0	1.2 – 1.5	67.18	1.33	–0.011	17.7	1.0	1.6
63.5 – 71.0	1.5 – 2.0	67.18	1.69	–0.019	6.25	0.20	0.43
63.5 – 71.0	2.0 – 2.8	67.18	2.24	–0.037	1.15	0.05	0.08
63.5 – 71.0	2.8 – 4.0	67.18	3.09	–0.072	0.081	0.012	0.005
71.0 – 79.3	0.9 – 1.1	75.07	0.97	–0.001	44.0	1.6	4.1
71.0 – 79.3	1.1 – 1.2	75.07	1.12	–0.004	29.6	0.9	2.6
71.0 – 79.3	1.2 – 1.5	75.07	1.33	–0.007	16.00	0.48	1.40
71.0 – 79.3	1.5 – 2.0	75.07	1.69	–0.015	5.23	0.17	0.46
71.0 – 79.3	2.0 – 2.8	75.07	2.24	–0.030	1.02	0.05	0.07
71.0 – 79.3	2.8 – 4.0	75.07	3.10	–0.063	0.069	0.009	0.005
79.3 – 88.5	1.1 – 1.2	83.81	1.12	–0.001	25.1	1.1	2.3
79.3 – 88.5	1.2 – 1.5	83.81	1.33	–0.004	14.64	0.46	1.30
79.3 – 88.5	1.5 – 2.0	83.81	1.69	–0.011	4.75	0.16	0.42
79.3 – 88.5	2.0 – 2.8	83.81	2.25	–0.025	0.93	0.04	0.07
79.3 – 88.5	2.8 – 4.0	83.81	3.11	–0.054	0.069	0.008	0.005
88.5 – 98.7	1.2 – 1.5	93.50	1.33	–0.001	13.43	0.49	1.21
88.5 – 98.7	1.5 – 2.0	93.50	1.69	–0.007	4.41	0.46	0.39
88.5 – 98.7	2.0 – 2.8	93.50	2.25	–0.019	0.81	0.04	0.06
88.5 – 98.7	2.8 – 4.0	93.50	3.11	–0.046	0.064	0.011	0.004
98.7 – 110.0	1.2 – 1.5	104.23	1.33	+0.003	10.8	1.5	1.0
98.7 – 110.0	1.5 – 2.0	104.23	1.69	–0.003	3.83	0.69	0.34
98.7 – 110.0	2.0 – 2.8	104.23	2.25	–0.014	0.68	0.07	0.06
98.7 – 110.0	2.8 – 4.0	104.23	3.12	–0.038	0.052	0.008	0.003

References

- [1] T. K. Gaisser and E. H. Levy, *Astrophysical implications of cosmic-ray antiprotons*, Phys. Rev. **D10** (1974) 1731.
- [2] G. Steigman, *Observational tests of antimatter cosmologies*, Ann. Rev. Astron. Astrophys. **14** (1976) 339.
- [3] J. Silk and M. Srednicki, *Cosmic-ray antiprotons as a probe of a photino-dominated Universe*, Phys. Rev. Lett. **53** (1984) 624.

- [4] F. W. Stecker, S. Rudaz, and T. F. Walsh, *Galactic antiprotons from photinos*, Phys. Rev. Lett. **55** (1985) 2622.
- [5] J. S. Hagelin and G. L. Kane, *Cosmic ray antimatter from supersymmetric dark matter*, Nucl. Phys. **B263** (1986) 399.
- [6] PAMELA collaboration, O. Adriani *et al.*, *Measurement of the flux of primary cosmic ray antiprotons with energies of 60 MeV to 350 GeV in the PAMELA experiment*, JETP Letters **96** (2013) 621.
- [7] AMS collaboration, M. Aguilar *et al.*, *Antiproton flux, antiproton-to-proton flux ratio, and properties of elementary particle fluxes in primary cosmic rays measured with the Alpha Magnetic Spectrometer on the International Space Station*, Phys. Rev. Lett. **117** (2016) 091103.
- [8] M. di Mauro, F. Donato, A. Goudelis, and P. D. Serpico, *New evaluation of the antiproton production cross section for cosmic ray studies*, Phys. Rev. **D90** (2014) 085017, [arXiv:1408.0288](#).
- [9] G. Giesen *et al.*, *AMS-02 antiprotons, at last! Secondary astrophysical component and immediate implications for dark matter*, JCAP **09** (2015) 023, [arXiv:1504.04276](#).
- [10] R. Kappl, A. Reinert, and M. W. Winkler, *AMS-02 antiprotons reloaded*, JCAP **10** (2015) 034, [arXiv:1506.04145](#).
- [11] A. Reinert and M. W. Winkler, *A precision search for WIMPs with charged cosmic rays*, JCAP **1801** (2018) 055, [arXiv:1712.00002](#).
- [12] F. Donato, M. Korsmeier, and M. Di Mauro, *Prescriptions on antiproton cross section data for precise theoretical antiproton flux predictions*, Phys. Rev. **D96** (2017) 043007, [arXiv:1704.03663](#).
- [13] LHCb collaboration, A. A. Alves Jr. *et al.*, *The LHCb detector at the LHC*, JINST **3** (2008) S08005.
- [14] LHCb collaboration, R. Aaij *et al.*, *LHCb detector performance*, Int. J. Mod. Phys. **A30** (2015) 1530022, [arXiv:1412.6352](#).
- [15] M. Adinolfi *et al.*, *Performance of the LHCb RICH detector at the LHC*, Eur. Phys. J. **C73** (2013) 2431, [arXiv:1211.6759](#).
- [16] C. Barschel, *Precision luminosity measurement at LHCb with beam-gas imaging*, PhD thesis, RWTH Aachen U., 2014, CERN-THESIS-2013-301.
- [17] LHCb collaboration, R. Aaij *et al.*, *Precision luminosity measurements at LHCb*, JINST **9** (2014) P12005, [arXiv:1410.0149](#).
- [18] L. Evans and P. Bryant, *LHC Machine*, JINST **3** (2008) S08001.
- [19] T. Pierog *et al.*, *EPOS LHC: test of collective hadronization with data measured at the CERN Large Hadron Collider*, Phys. Rev. **C92** (2015) 034906, [arXiv:1306.0121](#).

- [20] A. V. Gramolin *et al.*, *A new event generator for the elastic scattering of charged leptons on protons*, J. Phys. **G41** (2014) 115001, [arXiv:1401.2959](#).
- [21] Geant4 collaboration, J. Allison *et al.*, *Geant4 developments and applications*, IEEE Trans. Nucl. Sci. **53** (2006) 270; Geant4 collaboration, S. Agostinelli *et al.*, *Geant4: A simulation toolkit*, Nucl. Instrum. Meth. **A506** (2003) 250.
- [22] M. Clemencic *et al.*, *The LHCb simulation application, Gauss: Design, evolution and experience*, J. Phys. Conf. Ser. **331** (2011) 032023.
- [23] LHCb collaboration, R. Aaij *et al.*, *Measurement of the track reconstruction efficiency at LHCb*, JINST **10** (2015) P02007, [arXiv:1408.1251](#).
- [24] LHCb collaboration, R. Aaij *et al.*, *Measurement of prompt hadron production ratios in pp collisions at $\sqrt{s} = 0.9$ and 7 TeV*, Eur. Phys. J. **C72** (2012) 2168, [arXiv:1206.5160](#).
- [25] Y. Freund and R. E. Schapire, *A decision-theoretic generalization of on-line learning and an application to boosting*, J. Comput. Syst. Sci. **55** (1997) 119.
- [26] T. Pierog and K. Werner, *EPOS model and ultra high energy cosmic rays*, Nucl. Phys. Proc. Suppl. **196** (2009) 102, [arXiv:0905.1198](#).
- [27] M. Gyulassy and X.-N. Wang, *HIJING 1.0: A Monte Carlo program for parton and particle production in high-energy hadronic and nuclear collisions*, Comput. Phys. Commun. **83** (1994) 307, [arXiv:nucl-th/9502021](#).
- [28] S. Ostapchenko, *Monte Carlo treatment of hadronic interactions in enhanced Pomeron scheme: QGSJET-II model*, Phys. Rev. **D83** (2011) 014018, [arXiv:1010.1869](#).
- [29] M. Kachelriess, I. V. Moskalenko, and S. S. Ostapchenko, *New calculation of antiproton production by cosmic ray protons and nuclei*, Astrophys. J. **803** (2015) 54, [arXiv:1502.04158](#).
- [30] T. Sjöstrand, S. Mrenna, and P. Skands, *PYTHIA 6.4 physics and manual*, JHEP **05** (2006) 026, [arXiv:hep-ph/0603175](#).
- [31] M. Korsmeier, F. Donato, and M. Di Mauro, *Production cross sections of cosmic antiprotons in the light of new data from the NA61 and LHCb experiments*, Phys. Rev. D **97** (2018) 103019, [arXiv:1802.03030](#).

LHCb collaboration

R. Aaij²⁸, C. Abellán Beteta⁴⁵, B. Adeva⁴², M. Adinolfi⁴⁹, C.A. Aidala⁷⁴, Z. Ajaltouni⁵, S. Akar⁶⁰, P. Albicocco¹⁹, J. Albrecht¹⁰, F. Alessio⁴³, M. Alexander⁵⁴, A. Alfonso Alberio⁴¹, G. Alkhazov³⁴, P. Alvarez Cartelle⁵⁶, A.A. Alves Jr⁴², S. Amato², S. Amerio²⁴, Y. Amhis⁷, L. An³, L. Anderlini¹⁷, G. Andreassi⁴⁴, M. Andreotti¹⁶, J.E. Andrews⁶¹, R.B. Appleby⁵⁷, F. Archilli²⁸, P. d'Argent¹², J. Arnau Romeu⁶, A. Artamonov⁴⁰, M. Artuso⁶², K. Arzymatov³⁸, E. Aslanides⁶, M. Atzeni⁴⁵, B. Audurier²³, S. Bachmann¹², J.J. Back⁵¹, S. Baker⁵⁶, V. Balagura^{7,b}, W. Baldini¹⁶, A. Baranov³⁸, R.J. Barlow⁵⁷, S. Barsuk⁷, W. Barter⁵⁷, F. Baryshnikov⁷¹, V. Batozskaya³², B. Batsukh⁶², V. Battista⁴⁴, A. Bay⁴⁴, J. Beddow⁵⁴, F. Bedeschi²⁵, I. Bediaga¹, A. Beiter⁶², L.J. Bel²⁸, S. Belin²³, N. Bely⁶⁴, V. Bellec⁴⁴, N. Belloli^{21,i}, K. Belous⁴⁰, I. Belyaev^{35,43}, E. Ben-Haim⁸, G. Bencivenni¹⁹, S. Benson²⁸, S. Beranek⁹, A. Berezhnoy³⁶, R. Bernet⁴⁵, D. Berninghoff¹², E. Bertholet⁸, A. Bertolin²⁴, C. Betancourt⁴⁵, F. Betti^{15,43}, M.O. Bettler⁵⁰, M. van Beuzekom²⁸, I.a. Bezshyiko⁴⁵, S. Bhasin⁴⁹, J. Bhom³⁰, S. Bifani⁴⁸, P. Billoir⁸, A. Birnkraut¹⁰, A. Bizzeti^{17,u}, M. Bjørn⁵⁸, M.P. Blago⁴³, T. Blake⁵¹, F. Blanc⁴⁴, S. Blusk⁶², D. Bobulska⁵⁴, V. Bocci²⁷, O. Boente Garcia⁴², T. Boettcher⁵⁹, A. Bondar^{39,w}, N. Bondar³⁴, S. Borghi^{57,43}, M. Borisyak³⁸, M. Borsato⁴², F. Bossu⁷, M. Boubdir⁹, T.J.V. Bowcock⁵⁵, C. Bozzi^{16,43}, S. Braun¹², M. Brodski⁴³, J. Brodzicka³⁰, A. Brossa Gonzalo⁵¹, D. Brundu²³, E. Buchanan⁴⁹, A. Buonauro⁴⁵, C. Buri⁵⁷, A. Bursche²³, J. Buytaert⁴³, W. Byczynski⁴³, S. Cadeddu²³, H. Cai⁶⁵, R. Calabrese^{16,g}, R. Calladine⁴⁸, M. Calvi^{21,i}, M. Calvo Gomez^{41,m}, A. Camboni^{41,m}, P. Campana¹⁹, D.H. Campora Perez⁴³, L. Capriotti¹⁵, A. Carbone^{15,e}, G. Carboni²⁶, R. Cardinale^{20,h}, A. Cardini²³, P. Carniti^{21,i}, L. Carson⁵³, K. Carvalho Akiba², G. Casse⁵⁵, L. Cassina²¹, M. Cattaneo⁴³, G. Cavallero^{20,h}, R. Cenci^{25,p}, D. Chamont⁷, M.G. Chapman⁴⁹, M. Charles⁸, Ph. Charpentier⁴³, G. Chatzikonstantinidis⁴⁸, M. Chefdeville⁴, V. Chekalina³⁸, C. Chen³, S. Chen²³, S.-G. Chitic⁴³, V. Chobanova⁴², M. Chruszcz⁴³, A. Chubykin³⁴, P. Ciambrone¹⁹, X. Cid Vidal⁴², G. Ciezarek⁴³, P.E.L. Clarke⁵³, M. Clemencic⁴³, H.V. Cliff⁵⁰, J. Closier⁴³, V. Coco⁴³, J.A.B. Coelho⁷, J. Cogan⁶, E. Cogneras⁵, L. Cojocariu³³, P. Collins⁴³, T. Colombo⁴³, A. Comerma-Montells¹², A. Contu²³, G. Coombs⁴³, S. Coquereau⁴¹, G. Corti⁴³, M. Corvo^{16,g}, C.M. Costa Sobral⁵¹, B. Couturier⁴³, G.A. Cowan⁵³, D.C. Craik⁵⁹, A. Crocombe⁵¹, M. Cruz Torres¹, R. Currie⁵³, C. D'Ambrosio⁴³, F. Da Cunha Marinho², C.L. Da Silva⁷⁵, E. Dall'Occo²⁸, J. Dalseno⁴⁹, A. Danilina³⁵, A. Davis³, O. De Aguiar Francisco⁴³, K. De Bruyn⁴³, S. De Capua⁵⁷, M. De Cian⁴⁴, J.M. De Miranda¹, L. De Paula², M. De Serio^{14,d}, P. De Simone¹⁹, C.T. Dean⁵⁴, D. Decamp⁴, L. Del Buono⁸, B. Delaney⁵⁰, H.-P. Dembinski¹¹, M. Demmer¹⁰, A. Dendek³¹, D. Derkach³⁸, O. Deschamps⁵, F. Desse⁷, F. Dettori⁵⁵, B. Dey⁶⁶, A. Di Canto⁴³, P. Di Nezza¹⁹, S. Didenko⁷¹, H. Dijkstra⁴³, F. Dordei⁴³, M. Dorigo^{43,y}, A. Dosil Suárez⁴², L. Douglas⁵⁴, A. Dovbnya⁴⁶, K. Dreimanis⁵⁵, L. Dufour²⁸, G. Dujany⁸, P. Durante⁴³, J.M. Durham⁷⁵, D. Dutta⁵⁷, R. Dzhelyadin⁴⁰, M. Dziwiecki¹², A. Dziurda³⁰, A. Dzyuba³⁴, S. Easo⁵², U. Egede⁵⁶, V. Egorychev³⁵, S. Eidelman^{39,w}, S. Eisenhardt⁵³, U. Eitschberger¹⁰, R. Ekelhof¹⁰, L. Eklund⁵⁴, S. Ely⁶², A. Ene³³, S. Escher⁹, S. Esen²⁸, T. Evans⁶⁰, A. Falabella¹⁵, N. Farley⁴⁸, S. Farry⁵⁵, D. Fazzini^{21,43,i}, L. Federici²⁶, P. Fernandez Declara⁴³, A. Fernandez Prieto⁴², F. Ferrari¹⁵, L. Ferreira Lopes⁴⁴, F. Ferreira Rodrigues², M. Ferro-Luzzi⁴³, S. Filippov³⁷, R.A. Fini¹⁴, M. Fiorini^{16,g}, M. Firlej³¹, C. Fitzpatrick⁴⁴, T. Fiutowski³¹, F. Fleuret^{7,b}, M. Fontana^{23,43}, F. Fontanelli^{20,h}, R. Forty⁴³, V. Franco Lima⁵⁵, M. Frank⁴³, C. Frei⁴³, J. Fu^{22,q}, W. Funk⁴³, C. Färber⁴³, M. Féo Pereira Rivello Carvalho²⁸, E. Gabriel⁵³, A. Gallas Torreira⁴², D. Galli^{15,e}, S. Gallorini²⁴, S. Gambetta⁵³, Y. Gan³, M. Gandelman², P. Gandini²², Y. Gao³, L.M. Garcia Martin⁷³, B. Garcia Plana⁴², J. García Pardiñas⁴⁵, J. Garra Tico⁵⁰, L. Garrido⁴¹, D. Gascon⁴¹, C. Gaspar⁴³, L. Gavardi¹⁰, G. Gazzoni⁵, D. Gerick¹², E. Gersabeck⁵⁷, M. Gersabeck⁵⁷, T. Gershon⁵¹, D. Gerstel⁶, Ph. Ghez⁴, S. Gianì⁴⁴, V. Gibson⁵⁰, O.G. Girard⁴⁴, L. Giubega³³,

K. Gizdov⁵³, V.V. Gligorov⁸, D. Golubkov³⁵, A. Golutvin^{56,71}, A. Gomes^{1,a}, I.V. Gorelov³⁶,
 C. Gotti^{21,i}, E. Govorkova²⁸, J.P. Grabowski¹², R. Graciani Diaz⁴¹, L.A. Granado Cardoso⁴³,
 E. Graugés⁴¹, E. Graverini⁴⁵, G. Graziani¹⁷, A. Grecu³³, R. Greim²⁸, P. Griffith²³, L. Grillo⁵⁷,
 L. Gruber⁴³, B.R. Gruberg Cazon⁵⁸, O. Grünberg⁶⁸, C. Gu³, E. Gushchin³⁷, Yu. Guz^{40,43},
 T. Gys⁴³, C. Göbel⁶³, T. Hadavizadeh⁵⁸, C. Hadjivasiliou⁵, G. Haefeli⁴⁴, C. Haen⁴³,
 S.C. Haines⁵⁰, B. Hamilton⁶¹, X. Han¹², T.H. Hancock⁵⁸, S. Hansmann-Menzemer¹²,
 N. Harnew⁵⁸, S.T. Harnew⁴⁹, T. Harrison⁵⁵, C. Hasse⁴³, M. Hatch⁴³, J. He⁶⁴, M. Hecker⁵⁶,
 K. Heinicke¹⁰, A. Heister¹⁰, K. Hennessy⁵⁵, L. Henry⁷³, E. van Herwijnen⁴³, M. Heß⁶⁸,
 A. Hicheur², R. Hidalgo Charman⁵⁷, D. Hill⁵⁸, M. Hilton⁵⁷, P.H. Hopchev⁴⁴, W. Hu⁶⁶,
 W. Huang⁶⁴, Z.C. Huard⁶⁰, W. Hulsbergen²⁸, T. Humair⁵⁶, M. Hushchyn³⁸, D. Hutchcroft⁵⁵,
 D. Hynds²⁸, P. Ibis¹⁰, M. Idzik³¹, P. Ilten⁴⁸, K. Ivshin³⁴, R. Jacobsson⁴³, J. Jalocha⁵⁸,
 E. Jans²⁸, A. Jawahery⁶¹, F. Jiang³, M. John⁵⁸, D. Johnson⁴³, C.R. Jones⁵⁰, C. Joram⁴³,
 B. Jost⁴³, N. Jurik⁵⁸, S. Kandybei⁴⁶, M. Karacson⁴³, J.M. Kariuki⁴⁹, S. Karodia⁵⁴, N. Kazeev³⁸,
 M. Kecke¹², F. Keizer⁵⁰, M. Kelsey⁶², M. Kenzie⁵⁰, T. Ketel²⁹, E. Khairullin³⁸, B. Khanji⁴³,
 C. Khurewathanakul⁴⁴, K.E. Kim⁶², T. Kirn⁹, S. Klaver¹⁹, K. Klimaszewski³², T. Klimkovich¹¹,
 S. Koliiev⁴⁷, M. Kolpin¹², R. Kopečna¹², P. Koppenburg²⁸, I. Kostiuik²⁸, S. Kotriakhova³⁴,
 M. Kozeiha⁵, L. Kravchuk³⁷, M. Kreps⁵¹, F. Kress⁵⁶, P. Krokovny^{39,w}, W. Krupa³¹,
 W. Krzemien³², W. Kucewicz^{30,l}, M. Kucharczyk³⁰, V. Kudryavtsev^{39,w}, A.K. Kuonen⁴⁴,
 T. Kvaratskheliya^{35,43}, D. Lacarrere⁴³, G. Lafferty⁵⁷, A. Lai²³, D. Lancierini⁴⁵, G. Lanfranchi¹⁹,
 C. Langenbruch⁹, T. Latham⁵¹, C. Lazzeroni⁴⁸, R. Le Gac⁶, A. Leflat³⁶, J. Lefrançois⁷,
 R. Lefèvre⁵, F. Lemaître⁴³, O. Leroy⁶, T. Lesiak³⁰, B. Leverington¹², P.-R. Li⁶⁴, T. Li³, Z. Li⁶²,
 X. Liang⁶², T. Likhomanenko⁷⁰, R. Lindner⁴³, F. Lionetto⁴⁵, V. Lisovskyi⁷, X. Liu³, D. Loh⁵¹,
 A. Loi²³, I. Longstaff⁵⁴, J.H. Lopes², G.H. Lovell⁵⁰, C. Lucarelli¹⁸, D. Lucchesi^{24,o},
 M. Lucio Martinez⁴², A. Lupato²⁴, E. Luppi^{16,g}, O. Lupton⁴³, A. Lusiani²⁵, X. Lyu⁶⁴,
 F. Machefert⁷, F. Maciuc³³, V. Macko⁴⁴, P. Mackowiak¹⁰, S. Maddrell-Mander⁴⁹, O. Maev^{34,43},
 K. Maguire⁵⁷, D. Maisuzenko³⁴, M.W. Majewski³¹, S. Malde⁵⁸, B. Malecki³⁰, A. Malinin⁷⁰,
 T. Maltsev^{39,w}, G. Manca^{23,f}, G. Mancinelli⁶, D. Marangotto^{22,q}, J. Maratas^{5,v}, J.F. Marchand⁴,
 U. Marconi¹⁵, S. Mariani¹⁸, C. Marin Benito⁷, M. Marinangeli⁴⁴, P. Marino⁴⁴, J. Marks¹²,
 P.J. Marshall⁵⁵, G. Martellotti²⁷, M. Martin⁶, M. Martinelli⁴³, D. Martinez Santos⁴²,
 F. Martinez Vidal⁷³, A. Massafferri¹, M. Materok⁹, R. Matev⁴³, A. Mathad⁵¹, Z. Mathe⁴³,
 C. Matteuzzi²¹, A. Mauri⁴⁵, E. Maurice^{7,b}, B. Maurin⁴⁴, A. Mazurov⁴⁸, M. McCann^{56,43},
 A. McNab⁵⁷, R. McNulty¹³, J.V. Mead⁵⁵, B. Meadows⁶⁰, C. Meaux⁶, F. Meier¹⁰, N. Meinert⁶⁸,
 D. Melnychuk³², M. Merk²⁸, A. Merli^{22,q}, E. Michielin²⁴, D.A. Milanese⁶⁷, E. Millard⁵¹,
 M.-N. Minard⁴, L. Minzoni^{16,g}, D.S. Mitzel¹², A. Mogini⁸, J. Molina Rodriguez^{1,z},
 T. Mombächer¹⁰, I.A. Monroy⁶⁷, S. Monteil⁵, M. Morandin²⁴, G. Morello¹⁹, M.J. Morello^{25,t},
 O. Morgunova⁷⁰, J. Moron³¹, A.B. Morris⁶, R. Mountain⁶², F. Muheim⁵³, M. Mulder²⁸,
 C.H. Murphy⁵⁸, D. Murray⁵⁷, A. Mödden¹⁰, D. Müller⁴³, J. Müller¹⁰, K. Müller⁴⁵, V. Müller¹⁰,
 P. Naik⁴⁹, T. Nakada⁴⁴, R. Nandakumar⁵², A. Nandi⁵⁸, T. Nanut⁴⁴, I. Nasteva², M. Needham⁵³,
 N. Neri²², S. Neubert¹², N. Neufeld⁴³, M. Neuner¹², R. Newcombe⁵⁶, T.D. Nguyen⁴⁴,
 C. Nguyen-Mau^{44,n}, S. Nieswand⁹, R. Niet¹⁰, N. Nikitin³⁶, A. Nogay⁷⁰, N.S. Nolte⁴³,
 D.P. O'Hanlon¹⁵, A. Oblakowska-Mucha³¹, V. Obraztsov⁴⁰, S. Ogilvy¹⁹, R. Oldeman^{23,f},
 C.J.G. Onderwater⁶⁹, A. Ossowska³⁰, J.M. Otalora Goicochea², P. Owen⁴⁵, A. Oyanguren⁷³,
 P.R. Pais⁴⁴, T. Pajero^{25,t}, A. Palano¹⁴, M. Palutan^{19,43}, G. Panshin⁷², A. Papanestis⁵²,
 M. Pappagallo⁵³, L.L. Pappalardo^{16,g}, W. Parker⁶¹, C. Parkes⁵⁷, G. Passaleva^{17,43}, A. Pastore¹⁴,
 M. Patel⁵⁶, C. Patrignani^{15,e}, A. Pearce⁴³, A. Pellegrino²⁸, G. Penso²⁷, M. Pepe Altarelli⁴³,
 S. Perazzini⁴³, D. Pereima³⁵, P. Perret⁵, L. Pescatore⁴⁴, K. Petridis⁴⁹, A. Petrolini^{20,h},
 A. Petrov⁷⁰, S. Petrucci⁵³, M. Petruzzio^{22,q}, B. Pietrzyk⁴, G. Pietrzyk⁴⁴, M. Piques³⁰, M. Pili⁵⁸,
 D. Pinci²⁷, J. Pinzino⁴³, F. Pisani⁴³, A. Piucci¹², V. Placinta³³, S. Playfer⁵³, J. Plews⁴⁸,
 M. Plo Casasus⁴², F. Polci⁸, M. Poli Lener¹⁹, A. Poluektov⁵¹, N. Polukhina^{71,c}, I. Polyakov⁶²,
 E. Polcarpo², G.J. Pomery⁴⁹, S. Ponce⁴³, A. Popov⁴⁰, D. Popov^{48,11}, S. Poslavskii⁴⁰,

C. Potterat², E. Price⁴⁹, J. Prisciandaro⁴², C. Prouve⁴⁹, V. Pugatch⁴⁷, A. Puig Navarro⁴⁵, H. Pullen⁵⁸, G. Punzi^{25,p}, W. Qian⁶⁴, J. Qin⁶⁴, R. Quagliani⁸, B. Quintana⁵, B. Rachwal³¹, J.H. Rademacker⁴⁹, M. Rama²⁵, M. Ramos Pernas⁴², M.S. Rangel², F. Ratnikov^{38,x}, G. Raven²⁹, M. Ravonel Salzgeber⁴³, M. Reboud⁴, F. Redi⁴⁴, S. Reichert¹⁰, A.C. dos Reis¹, F. Reiss⁸, C. Remon Alepuz⁷³, Z. Ren³, V. Renaudin⁷, S. Ricciardi⁵², S. Richards⁴⁹, K. Rinnert⁵⁵, P. Robbe⁷, A. Robert⁸, A.B. Rodrigues⁴⁴, E. Rodrigues⁶⁰, J.A. Rodriguez Lopez⁶⁷, M. Roehrken⁴³, S. Roiser⁴³, A. Rollings⁵⁸, V. Romanovskiy⁴⁰, A. Romero Vidal⁴², M. Rotondo¹⁹, M.S. Rudolph⁶², T. Ruf⁴³, J. Ruiz Vidal⁷³, J.J. Saborido Silva⁴², N. Sagidova³⁴, B. Saitta^{23,f}, V. Salustino Guimaraes⁶³, C. Sanchez Gras²⁸, C. Sanchez Mayordomo⁷³, B. Sanmartin Sedes⁴², R. Santacesaria²⁷, C. Santamarina Rios⁴², M. Santimaria¹⁹, E. Santovetti^{26,j}, G. Sarpis⁵⁷, A. Sarti^{19,k}, C. Satriano^{27,s}, A. Satta²⁶, M. Saur⁶⁴, D. Savrina^{35,36}, S. Schael⁹, M. Schellenberg¹⁰, M. Schiller⁵⁴, H. Schindler⁴³, M. Schmelling¹¹, T. Schmelzer¹⁰, B. Schmidt⁴³, O. Schneider⁴⁴, A. Schopper⁴³, H.F. Schreiner⁶⁰, M. Schubiger⁴⁴, M.H. Schune⁷, R. Schwemmer⁴³, B. Sciascia¹⁹, A. Sciubba^{27,k}, A. Semennikov³⁵, E.S. Sepulveda⁸, A. Sergi^{48,43}, N. Serra⁴⁵, J. Serrano⁶, L. Sestini²⁴, A. Seuthe¹⁰, P. Seyfert⁴³, M. Shapkin⁴⁰, Y. Shcheglov^{34,†}, T. Shears⁵⁵, L. Shekhtman^{39,w}, V. Shevchenko⁷⁰, E. Shmanin⁷¹, B.G. Siddi¹⁶, R. Silva Coutinho⁴⁵, L. Silva de Oliveira², G. Simi^{24,o}, S. Simone^{14,d}, I. Skiba¹⁶, N. Skidmore¹², T. Skwarnicki⁶², M.W. Slater⁴⁸, J.G. Smeaton⁵⁰, E. Smith⁹, I.T. Smith⁵³, M. Smith⁵⁶, M. Soares¹⁵, I. Soares Lavra¹, M.D. Sokoloff⁶⁰, F.J.P. Soler⁵⁴, B. Souza De Paula², B. Spaan¹⁰, E. Spadaro Norella^{22,q}, P. Spradlin⁵⁴, F. Stagni⁴³, M. Stahl¹², S. Stahl⁴³, P. Stefko⁴⁴, S. Stefkova⁵⁶, O. Steinkamp⁴⁵, S. Stemmler¹², O. Stenyakin⁴⁰, M. Stepanova³⁴, H. Stevens¹⁰, A. Stocchi⁷, S. Stone⁶², B. Storaci⁴⁵, S. Stracka²⁵, M.E. Stramaglia⁴⁴, M. Straticicuc³³, U. Straumann⁴⁵, S. Strokov⁷², J. Sun³, L. Sun⁶⁵, K. Swientek³¹, T. Szumlak³¹, M. Szymanski⁶⁴, S. T'Jampens⁴, Z. Tang³, A. Tayduganov⁶, T. Tekampe¹⁰, G. Tellarini¹⁶, F. Teubert⁴³, E. Thomas⁴³, J. van Tilburg²⁸, M.J. Tilley⁵⁶, V. Tisserand⁵, M. Tobin³¹, S. Tolk⁴³, L. Tomassetti^{16,g}, D. Tonelli²⁵, D.Y. Tou⁸, R. Tourinho Jadallah Aoude¹, E. Tournefier⁴, M. Traill⁵⁴, M.T. Tran⁴⁴, A. Trisovic⁵⁰, A. Tsaregorodtsev⁶, G. Tuci^{25,p}, A. Tully⁵⁰, N. Tuning^{28,43}, A. Ukleja³², A. Usachov⁷, A. Ustyuzhanin³⁸, U. Uwer¹², A. Vagner⁷², V. Vagnoni¹⁵, A. Valassi⁴³, S. Valat⁴³, G. Valenti¹⁵, R. Vazquez Gomez⁴³, P. Vazquez Regueiro⁴², S. Vecchi¹⁶, M. van Veghel²⁸, J.J. Velthuis⁴⁹, M. Veltri^{17,r}, G. Veneziano⁵⁸, A. Venkateswaran⁶², T.A. Verlage⁹, M. Vernet⁵, M. Veronesi²⁸, N.V. Veronika¹³, M. Vesterinen⁵⁸, J.V. Viana Barbosa⁴³, D. Vieira⁶⁴, M. Vieites Diaz⁴², H. Viemann⁶⁸, X. Vilasis-Cardona^{41,m}, A. Vitkovskiy²⁸, M. Vitti⁵⁰, V. Volkov³⁶, A. Vollhardt⁴⁵, D. Vom Bruch⁸, B. Voneki⁴³, A. Vorobyev³⁴, V. Vorobyev^{39,w}, J.A. de Vries²⁸, C. Vázquez Sierra²⁸, R. Waldi⁶⁸, J. Walsh²⁵, J. Wang⁶², M. Wang³, Y. Wang⁶⁶, Z. Wang⁴⁵, D.R. Ward⁵⁰, H.M. Wark⁵⁵, N.K. Watson⁴⁸, D. Websdale⁵⁶, A. Weiden⁴⁵, C. Weisser⁵⁹, M. Whitehead⁹, J. Wicht⁵¹, G. Wilkinson⁵⁸, M. Wilkinson⁶², I. Williams⁵⁰, M.R.J. Williams⁵⁷, M. Williams⁵⁹, T. Williams⁴⁸, F.F. Wilson^{52,43}, J. Wimberley⁶¹, M. Winn⁷, J. Wishahi¹⁰, W. Wislicki³², M. Witek³⁰, G. Wormser⁷, S.A. Wotton⁵⁰, K. Wyllie⁴³, D. Xiao⁶⁶, Y. Xie⁶⁶, A. Xu³, M. Xu⁶⁶, Q. Xu⁶⁴, Z. Xu³, Z. Xu⁴, Z. Yang³, Z. Yang⁶¹, Y. Yao⁶², L.E. Yeomans⁵⁵, H. Yin⁶⁶, J. Yu^{66,ab}, X. Yuan⁶², O. Yushchenko⁴⁰, K.A. Zarebski⁴⁸, M. Zavertyaev^{11,c}, D. Zhang⁶⁶, L. Zhang³, W.C. Zhang^{3,aa}, Y. Zhang⁷, A. Zhelezov¹², Y. Zheng⁶⁴, X. Zhu³, V. Zhukov^{9,36}, J.B. Zonneveld⁵³, S. Zucchelli¹⁵.

¹Centro Brasileiro de Pesquisas Físicas (CBPF), Rio de Janeiro, Brazil

²Universidade Federal do Rio de Janeiro (UFRJ), Rio de Janeiro, Brazil

³Center for High Energy Physics, Tsinghua University, Beijing, China

⁴Univ. Grenoble Alpes, Univ. Savoie Mont Blanc, CNRS, IN2P3-LAPP, Annecy, France

⁵Clermont Université, Université Blaise Pascal, CNRS/IN2P3, LPC, Clermont-Ferrand, France

⁶Aix Marseille Univ, CNRS/IN2P3, CPPM, Marseille, France

⁷LAL, Univ. Paris-Sud, CNRS/IN2P3, Université Paris-Saclay, Orsay, France

- ⁸LPNHE, Sorbonne Université, Paris Diderot Sorbonne Paris Cité, CNRS/IN2P3, Paris, France
- ⁹I. Physikalisches Institut, RWTH Aachen University, Aachen, Germany
- ¹⁰Fakultät Physik, Technische Universität Dortmund, Dortmund, Germany
- ¹¹Max-Planck-Institut für Kernphysik (MPIK), Heidelberg, Germany
- ¹²Physikalisches Institut, Ruprecht-Karls-Universität Heidelberg, Heidelberg, Germany
- ¹³School of Physics, University College Dublin, Dublin, Ireland
- ¹⁴INFN Sezione di Bari, Bari, Italy
- ¹⁵INFN Sezione di Bologna, Bologna, Italy
- ¹⁶INFN Sezione di Ferrara, Ferrara, Italy
- ¹⁷INFN Sezione di Firenze, Firenze, Italy
- ¹⁸Università di Firenze, Firenze, Italy
- ¹⁹INFN Laboratori Nazionali di Frascati, Frascati, Italy
- ²⁰INFN Sezione di Genova, Genova, Italy
- ²¹INFN Sezione di Milano-Bicocca, Milano, Italy
- ²²INFN Sezione di Milano, Milano, Italy
- ²³INFN Sezione di Cagliari, Monserrato, Italy
- ²⁴INFN Sezione di Padova, Padova, Italy
- ²⁵INFN Sezione di Pisa, Pisa, Italy
- ²⁶INFN Sezione di Roma Tor Vergata, Roma, Italy
- ²⁷INFN Sezione di Roma La Sapienza, Roma, Italy
- ²⁸Nikhef National Institute for Subatomic Physics, Amsterdam, Netherlands
- ²⁹Nikhef National Institute for Subatomic Physics and VU University Amsterdam, Amsterdam, Netherlands
- ³⁰Henryk Niewodniczanski Institute of Nuclear Physics Polish Academy of Sciences, Kraków, Poland
- ³¹AGH - University of Science and Technology, Faculty of Physics and Applied Computer Science, Kraków, Poland
- ³²National Center for Nuclear Research (NCBJ), Warsaw, Poland
- ³³Horia Hulubei National Institute of Physics and Nuclear Engineering, Bucharest-Magurele, Romania
- ³⁴Petersburg Nuclear Physics Institute (PNPI), Gatchina, Russia
- ³⁵Institute of Theoretical and Experimental Physics (ITEP), Moscow, Russia
- ³⁶Institute of Nuclear Physics, Moscow State University (SINP MSU), Moscow, Russia
- ³⁷Institute for Nuclear Research of the Russian Academy of Sciences (INR RAS), Moscow, Russia
- ³⁸Yandex School of Data Analysis, Moscow, Russia
- ³⁹Budker Institute of Nuclear Physics (SB RAS), Novosibirsk, Russia
- ⁴⁰Institute for High Energy Physics (IHEP), Protvino, Russia
- ⁴¹ICCUB, Universitat de Barcelona, Barcelona, Spain
- ⁴²Instituto Galego de Física de Altas Enerxías (IGFAE), Universidade de Santiago de Compostela, Santiago de Compostela, Spain
- ⁴³European Organization for Nuclear Research (CERN), Geneva, Switzerland
- ⁴⁴Institute of Physics, Ecole Polytechnique Fédérale de Lausanne (EPFL), Lausanne, Switzerland
- ⁴⁵Physik-Institut, Universität Zürich, Zürich, Switzerland
- ⁴⁶NSC Kharkiv Institute of Physics and Technology (NSC KIPT), Kharkiv, Ukraine
- ⁴⁷Institute for Nuclear Research of the National Academy of Sciences (KINR), Kyiv, Ukraine
- ⁴⁸University of Birmingham, Birmingham, United Kingdom
- ⁴⁹H.H. Wills Physics Laboratory, University of Bristol, Bristol, United Kingdom
- ⁵⁰Cavendish Laboratory, University of Cambridge, Cambridge, United Kingdom
- ⁵¹Department of Physics, University of Warwick, Coventry, United Kingdom
- ⁵²STFC Rutherford Appleton Laboratory, Didcot, United Kingdom
- ⁵³School of Physics and Astronomy, University of Edinburgh, Edinburgh, United Kingdom
- ⁵⁴School of Physics and Astronomy, University of Glasgow, Glasgow, United Kingdom
- ⁵⁵Oliver Lodge Laboratory, University of Liverpool, Liverpool, United Kingdom
- ⁵⁶Imperial College London, London, United Kingdom
- ⁵⁷School of Physics and Astronomy, University of Manchester, Manchester, United Kingdom
- ⁵⁸Department of Physics, University of Oxford, Oxford, United Kingdom
- ⁵⁹Massachusetts Institute of Technology, Cambridge, MA, United States
- ⁶⁰University of Cincinnati, Cincinnati, OH, United States

- ⁶¹ *University of Maryland, College Park, MD, United States*
⁶² *Syracuse University, Syracuse, NY, United States*
⁶³ *Pontifícia Universidade Católica do Rio de Janeiro (PUC-Rio), Rio de Janeiro, Brazil, associated to ²*
⁶⁴ *University of Chinese Academy of Sciences, Beijing, China, associated to ³*
⁶⁵ *School of Physics and Technology, Wuhan University, Wuhan, China, associated to ³*
⁶⁶ *Institute of Particle Physics, Central China Normal University, Wuhan, Hubei, China, associated to ³*
⁶⁷ *Departamento de Física, Universidad Nacional de Colombia, Bogota, Colombia, associated to ⁸*
⁶⁸ *Institut für Physik, Universität Rostock, Rostock, Germany, associated to ¹²*
⁶⁹ *Van Swinderen Institute, University of Groningen, Groningen, Netherlands, associated to ²⁸*
⁷⁰ *National Research Centre Kurchatov Institute, Moscow, Russia, associated to ³⁵*
⁷¹ *National University of Science and Technology "MISIS", Moscow, Russia, associated to ³⁵*
⁷² *National Research Tomsk Polytechnic University, Tomsk, Russia, associated to ³⁵*
⁷³ *Instituto de Física Corpuscular, Centro Mixto Universidad de Valencia - CSIC, Valencia, Spain, associated to ⁴¹*
⁷⁴ *University of Michigan, Ann Arbor, United States, associated to ⁶²*
⁷⁵ *Los Alamos National Laboratory (LANL), Los Alamos, United States, associated to ⁶²*

- ^a *Universidade Federal do Triângulo Mineiro (UFMG), Uberaba-MG, Brazil*
^b *Laboratoire Leprince-Ringuet, Palaiseau, France*
^c *P.N. Lebedev Physical Institute, Russian Academy of Science (LPI RAS), Moscow, Russia*
^d *Università di Bari, Bari, Italy*
^e *Università di Bologna, Bologna, Italy*
^f *Università di Cagliari, Cagliari, Italy*
^g *Università di Ferrara, Ferrara, Italy*
^h *Università di Genova, Genova, Italy*
ⁱ *Università di Milano Bicocca, Milano, Italy*
^j *Università di Roma Tor Vergata, Roma, Italy*
^k *Università di Roma La Sapienza, Roma, Italy*
^l *AGH - University of Science and Technology, Faculty of Computer Science, Electronics and Telecommunications, Kraków, Poland*
^m *LIFAEELS, La Salle, Universitat Ramon Llull, Barcelona, Spain*
ⁿ *Hanoi University of Science, Hanoi, Vietnam*
^o *Università di Padova, Padova, Italy*
^p *Università di Pisa, Pisa, Italy*
^q *Università degli Studi di Milano, Milano, Italy*
^r *Università di Urbino, Urbino, Italy*
^s *Università della Basilicata, Potenza, Italy*
^t *Scuola Normale Superiore, Pisa, Italy*
^u *Università di Modena e Reggio Emilia, Modena, Italy*
^v *MSU - Iligan Institute of Technology (MSU-IIT), Iligan, Philippines*
^w *Novosibirsk State University, Novosibirsk, Russia*
^x *National Research University Higher School of Economics, Moscow, Russia*
^y *Sezione INFN di Trieste, Trieste, Italy*
^z *Escuela Agrícola Panamericana, San Antonio de Oriente, Honduras*
^{aa} *School of Physics and Information Technology, Shaanxi Normal University (SNNU), Xi'an, China*
^{ab} *Physics and Micro Electronic College, Hunan University, Changsha City, China*

† *Deceased*